Article

Cell Reports

The Crystal Structure of the NHL Domain in Complex with RNA Reveals the Molecular Basis of *Drosophila* Brain-Tumor-Mediated Gene Regulation

Graphical Abstract

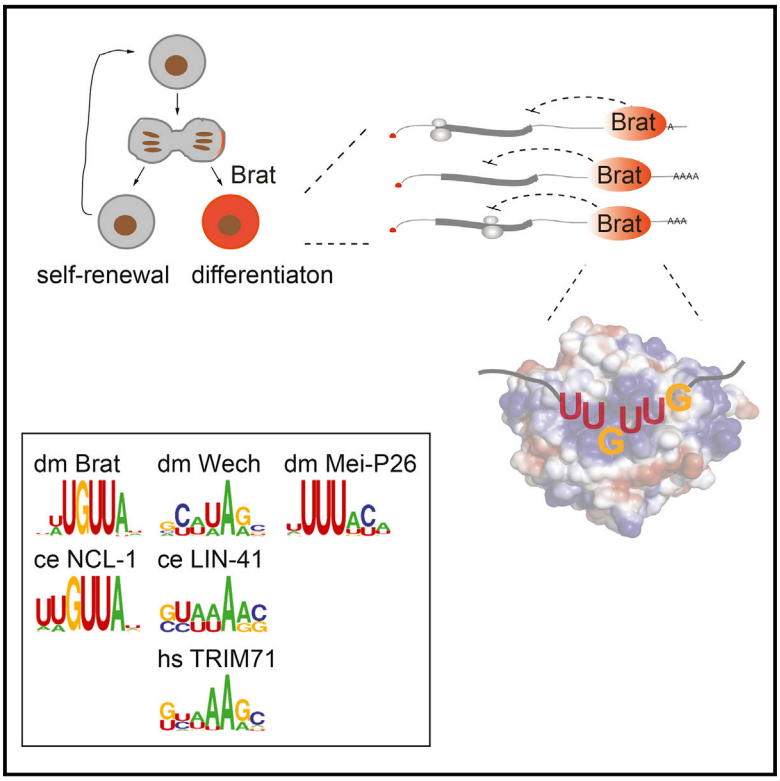

Authors

Inga Loedige, Leonhard Jakob, Thomas Treiber, ..., Julia C. Engelmann, Michael P. Krahn, Gunter Meister

Correspondence

inga.loedige@embl.de (I.L.), gunter.meister@ur.de (G.M.)

In Brief

TRIM-NHL proteins are important regulators of cell fate decisions and contact RNA targets via their NHL domains. In this study, Loedige et al. present the co-crystal structure of the NHL domain of *Drosophila* Brat in complex with its RNA-binding motif. This study reveals that NHL domains are widespread, sequence-specific RNA-binding modules.

Highlights

- The RNA-binding protein Brat binds several hundred mRNAs in *Drosophila* embryos
- Direct mRNA target binding is mediated by a highly specific RNA-binding motif
- X-ray crystallography uncovers the molecular basis of the Brat-RNA interaction
- NHL domains are RNA-binding modules with distinct RNA preferences

Accession Numbers

4ZLR
GSE71663
GSE73000

Loedige et al., 2015, Cell Reports *13*, 1206–1220
November 10, 2015 ©2015 The Authors
http://dx.doi.org/10.1016/j.celrep.2015.09.068

OPEN ACCESS
CellPress

Cell Reports
Article

The Crystal Structure of the NHL Domain in Complex with RNA Reveals the Molecular Basis of *Drosophila* Brain-Tumor-Mediated Gene Regulation

Inga Loedige,[1,*] Leonhard Jakob,[1] Thomas Treiber,[1] Debashish Ray,[2] Mathias Stotz,[1] Nora Treiber,[1] Janosch Hennig,[3,6] Kate B. Cook,[2] Quaid Morris,[2] Timothy R. Hughes,[2] Julia C. Engelmann,[4] Michael P. Krahn,[5] and Gunter Meister[1,*]

[1]Laboratory for RNA Biology, Biochemistry Center Regensburg, University of Regensburg, 93053 Regensburg, Germany
[2]Donnelly Centre for Cellular and Biomolecular Research, University of Toronto, Toronto M5S 3E1, Canada
[3]Group Biomolecular NMR, Institute of Structural Biology, Helmholtz Zentrum München, German Research Center for Environmental Health, 85764 Neuherberg, Germany
[4]Department of Statistical Bioinformatics, Institute for Functional Genomics, University of Regensburg, Josef-Engert-Straße 9, 93053 Regensburg, Germany
[5]Institute for Molecular and Cellular Anatomy, University of Regensburg, 93053 Regensburg, Germany
[6]Present address: Structural and Computational Biology Unit, EMBL Heidelberg, 69117 Heidelberg, Germany
*Correspondence: inga.loedige@embl.de (I.L.), gunter.meister@ur.de (G.M.)
http://dx.doi.org/10.1016/j.celrep.2015.09.068

SUMMARY

TRIM-NHL proteins are conserved among metazoans and control cell fate decisions in various stem cell linages. The *Drosophila* TRIM-NHL protein Brain tumor (Brat) directs differentiation of neuronal stem cells by suppressing self-renewal factors. Brat is an RNA-binding protein and functions as a translational repressor. However, it is unknown which RNAs Brat regulates and how RNA-binding specificity is achieved. Using RNA immunoprecipitation and RNAcompete, we identify Brat-bound mRNAs in *Drosophila* embryos and define consensus binding motifs for Brat as well as a number of additional TRIM-NHL proteins, indicating that TRIM-NHL proteins are conserved, sequence-specific RNA-binding proteins. We demonstrate that Brat-mediated repression and direct RNA-binding depend on the identified motif and show that binding of the localization factor Miranda to the Brat-NHL domain inhibits Brat activity. Finally, to unravel the sequence specificity of the NHL domain, we crystallize the Brat-NHL domain in complex with RNA and present a high-resolution protein-RNA structure of this fold.

INTRODUCTION

Eukaryotic gene expression programs are predominantly shaped by post-transcriptional mechanisms (Schwanhäusser et al., 2011). RNA-binding proteins (RBPs) interact with mRNAs to regulate their maturation, localization, translation, and decay. To understand post-transcriptional gene regulation, characterization of RBPs and their interaction networks is crucial. The development of large-scale methods has endorsed the systematic identification of RBPs as well as their target RNAs (Gerstberger et al., 2014). But despite these efforts, only a limited number of RNA-binding domains (RBDs) have been characterized to date, and our understanding of how binding selectivity and specificity is brought about or how different RBPs influence each other is still limited.

Post-transcriptional gene regulation plays important roles in controlling the balance between self-renewal and differentiation (Slaidina and Lehmann, 2014; Ye and Blelloch, 2014). Stem cells are characterized by their ability to self-renew and to produce differentiating progeny, generating cellular diversity during development and maintaining tissue homeostasis in adulthood. The switch between self-renewal and differentiation is tightly controlled, and its disruption can cause either premature differentiation and depletion of the stem cell pool or over-proliferation and tumor formation.

Drosophila melanogaster neuronal stem cells, termed neuroblasts (NBs), are one of the best understood model systems for stem cell biology, and many of the principles and regulatory mechanisms are conserved among species (Brand and Livesey, 2011; Gómez-López et al., 2014; Knoblich, 2010). Type II NBs divide asymmetrically to generate a self-renewing NB and a committed progenitor cell, termed intermediate neuronal progenitor (INP). INPs divide only a few more times before terminally differentiating. Cell fate determinants such as Numb, Prospero, and Brain tumor (Brat) are segregated into the differentiating daughter cell, where they inhibit self-renewal and promote differentiation. INPs that lack functional Brat, for example, fail to downregulate self-renewal factors, leading to an uncontrolled expansion of NBs and tumor formation (Betschinger et al., 2006; Lee et al., 2006). Two key components of the self-renewal network of type II NBs that are aberrantly expressed in INPs lacking Brat are the transcription factors Deadpan (Dpn) and Klumpfuss (Klu), and removal of either *dpn* or *klu* suppresses tumor formation in Brat-mutant flies (Janssens and Lee, 2014). The molecular details of how Brat represses their expression, however, remain elusive.

Brat belongs to the conserved family of TRIM-NHL proteins, which are characterized by their N-terminal tripartite motif

(TRIM), consisting of a RING domain, one or two B-box motifs, a coiled-coil region, and a C-terminal NCL-1, HT2A, LIN-41 (NHL) domain (Sardiello et al., 2008; Slack and Ruvkun, 1998; Figure 1A). Similar to Brat, several other TRIM-NHL proteins have been recognized as regulators of cell fate decisions in various stem or progenitor cell linages (Chang et al., 2012; Chen et al., 2014; Li et al., 2012; Neumüller et al., 2008; Schwamborn et al., 2009; Slack et al., 2000), including the mammalian Brat ortholog TRIM3, which has been identified as a tumor suppressor in glioblastoma (Chen et al., 2014; Liu et al., 2014), or human TRIM71, which facilitates reprogramming of differentiated cells in induced pluripotent stem cells (Worringer et al., 2014). Interestingly, the NHL domain of TRIM-NHL proteins has recently been shown to be an RBD (Kwon et al., 2013; Loedige et al., 2014).

In addition to its function during neurogenesis, Brat is also required for proper abdomen development in early embryos. Here Brat forms a complex with the RBPs Pumilio (Pum) and Nanos (Nos) to repress translation of the *hunchback* (*hb*) mRNA (Murata and Wharton, 1995; Sonoda and Wharton, 2001). Although it was initially thought that only Pum contacts the mRNA and recruits Brat and Nos via protein-protein interactions, we have recently demonstrated that Brat directly binds the *hb* RNA (Loedige et al., 2014). We identified Brat-binding sites that are distinct from the Pum consensus sequence and showed that RNA binding and Brat-mediated repression are independent of Pum. This strongly suggested the existence of Pum-independent Brat targets and a function for Brat RNA-binding in developmental processes that do not require Pum. Indeed, it has been shown recently that Brat-mediated repression of *src64B* mRNA, which is important for axon maintenance, is independent of Pum (Marchetti et al., 2014).

The NHL domain forms a six-bladed β propeller that is similar to the WD40 fold (Edwards et al., 2003), and its positively charged top surface contacts RNA (Loedige et al., 2014). However, the molecular details of this interaction, particularly how sequence specificity and selectivity are achieved, are unknown.

Here we combine genome-wide approaches, cell-based assays, biochemistry, and structural biology to provide a detailed molecular understanding of Brat-mediated post-transcriptional gene regulation. We systematically identify Brat-associated mRNAs, determine the Brat-binding motif, and crystallize the Brat-NHL domain in complex with a short RNA containing the identified motif at a resolution of 2.3 Å. Moreover, we define consensus RNA-binding motifs for different TRIM-NHL proteins, revealing that Brat is part of a conserved family of sequence-specific, single-stranded RBPs.

RESULTS

Identification of Brat-Associated mRNAs in Late-Stage *Drosophila* Embryos

To better understand the role of Brat in post-transcriptional gene expression, we sought to identify Brat-bound RNAs. We ubiquitously expressed FLAG-tagged Brat in fly embryos (Shi et al., 2013) and performed RNA immunoprecipitation (RIP) experiments followed by microarray analyses. Several hundred mRNAs were significantly enriched in the Brat-RIP, including the known Brat targets *diminutive* (*dm*) and *paralytic* (*para*), as well as many genes that are upregulated in brain tumors of Brat-mutant flies (Jüschke et al., 2013), such as *chinmo*, *dpn*, *klu*, *staufen* (*stau*), or *par-6* (Figure 1B). The enrichment of selected mRNAs was confirmed by qRT-PCR using RNA isolated from an independent experiment (Figure 1C). Consistently, all tested targets (except *cngl*) that were highly enriched in the microarray dataset were also enriched in the qRT-PCR analysis whereas mRNAs randomly chosen from the non-enriched pool were not.

Identification of a Brat Consensus Binding Motif

We have found previously that RNA-binding by Brat is sequence-specific (Loedige et al., 2014), and we therefore examined the 3′ UTRs of our top-ranking mRNA transcripts for the presence of a common motif using multiple expectation and maximization for motif elicitation (MEME) (Bailey and Elkan, 1994). MEME analysis revealed a 15-nt sequence encompassing a 6-nt core motif, UU[G/U]UU[G/A], followed by a U-rich stretch, as significantly enriched (Figure 1D). Additionally, we performed an in vitro selection experiment, referred to as RNAcompete (Ray et al., 2009, 2013), using the recombinant NHL domain of Brat and a complex pool of short RNAs. Consistent with the in vivo data, RNAcompete identified [U/A]UGUUA as the consensus binding sequence for Brat (Figure S1D). Consist with this, a recent study carried out in parallel to our work identified a highly similar Brat binding motif (Laver et al., 2015).

Computational analysis revealed a clear correlation between the enrichment of mRNAs in the Brat-RIP and the occurrence of the identified Brat-binding motif (Figure 1E), further validating our RIP data and the identified motif.

To further validate the Brat consensus motif and to determine binding affinities, we performed electrophoretic mobility shift assays (EMSAs) using the recombinant BRAT-NHL domain and short, 15-nt-long radiolabeled RNAs (15-mers) containing the identified binding motif or similar sequences embedded into a poly-U backbone (Figure 1F). Brat-NHL efficiently binds to the UUGUUG motif with an estimated affinity of 40 nM (I). Changing the second (II) or the first guanine (III) to an adenine only slightly reduced binding affinities (~40–80 nM). However, when the two guanines were located in the center of the poly-U RNA (IV) or when the second guanine was replaced by uracil (V), we observed a reduction in affinity. Finally, when poly-U was used as ligand (VI) or both guanines were changed to adenines (VII), affinity dropped below 160 nM. Therefore, we experimentally confirmed the identified binding motif, demonstrating that purines at positions 3 and 6 of the motif are required and that one of the two purines needs to be a guanine for high-affinity binding.

Crystal Structure of Brat-NHL in Complex with RNA

To elucidate the molecular contacts that define the identified binding motif, we crystallized the NHL domain of Brat bound to a short RNA containing the consensus UUGUUG motif at the 5′ end, followed by an oligo U stretch (nine Us). The refined structure at 2.3-Å resolution (Table S2) shows the NHL domain conformation to be almost unchanged in comparison with an unliganded structure reported before (Edwards et al., 2003). It is formed by a six-bladed β propeller that encloses a solvent-filled

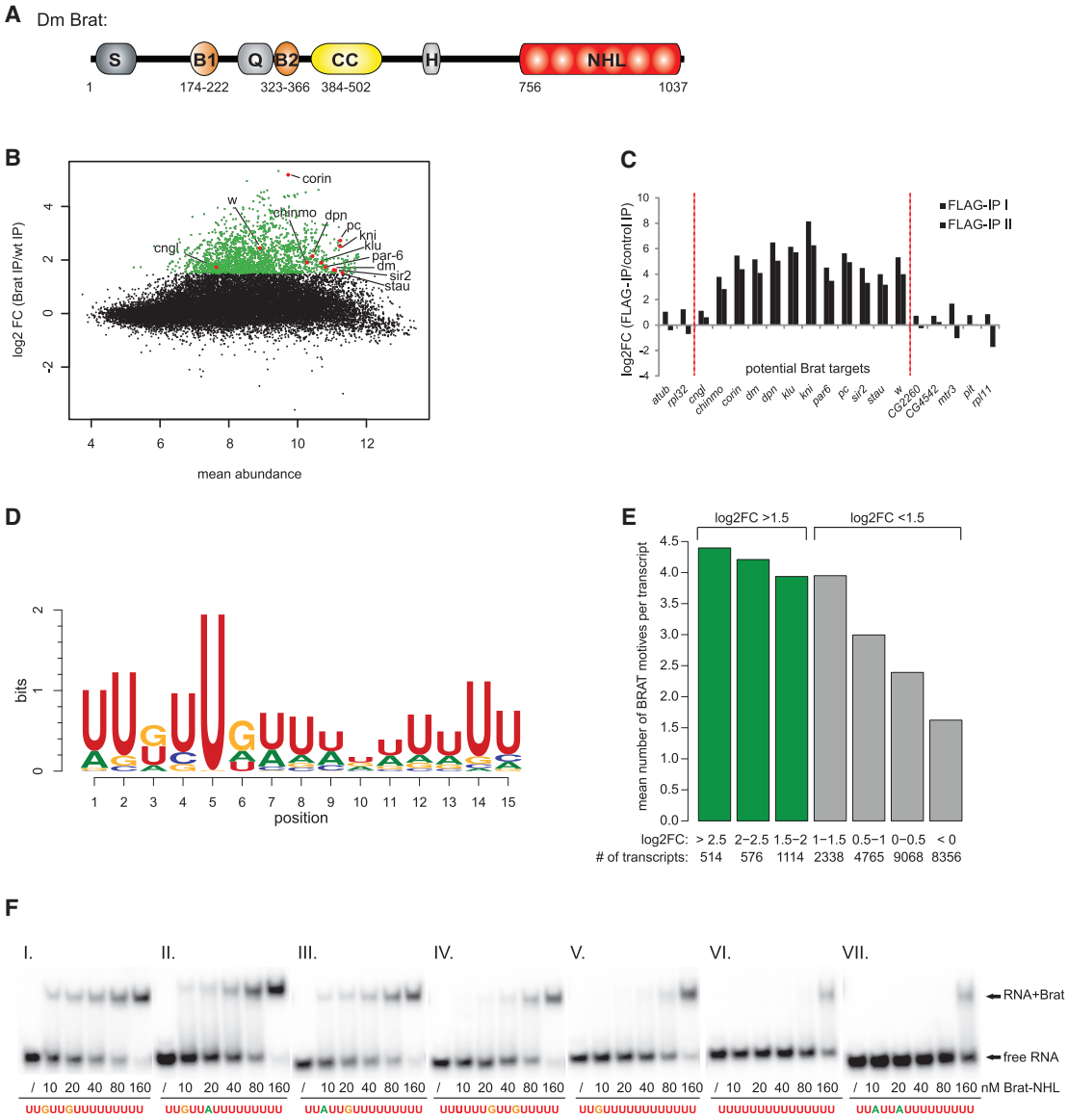

Figure 1. Identification of Brat-Associated mRNAs and a Brat Consensus Binding Motif

(A) Schematic of *Drosophila* (dm) Brat domain organization. Brat contains two B-boxes (B1 and B2, orange), a coiled-coil (CC) domain (yellow), and an NHL domain (red). Also shown are serine-rich (S), glutamine-rich (Q), and histidine-rich (H) stretches. Brat is only an incomplete TRIM because it lacks the RING domain. Numbers indicate domain boundaries.

(B) Brat binds several hundred mRNAs. Shown is an MA plot of RIP-Chip data showing the enrichment of transcripts versus their mean abundance. Enrichment was calculated as the ratio between Brat and control immunoprecipitation (IP). Transcripts enriched more than 2.8-fold (log2FC > 1.5, 2,204 transcripts corresponding to 953 genes) in the Brat IP are depicted in green. Transcripts selected for qRT-PCR validation are highlighted in red. Normalized microarray data are listed in Table S1.

(C) qRT-PCR validation of candidate Brat-targeted mRNAs. Shown is the relative enrichment of mRNAs in a Brat IP compared with a control IP. Western blots of lysates and IPs are shown in Figure S1.

(D) The Brat-binding motif. The sequence logo of the Brat consensus motif identified by MEME is shown.

(E) Enrichment of mRNAs in the Brat-RIP correlates with the number of Brat-binding sites. mRNA transcripts were divided into seven subsets according to their enrichment in the Brat IP. The average numbers of Brat-binding sites are shown as columns. Transcripts enriched more than 2.8-fold (log2FC > 1.5) in the Brat IP are shown in green.

(F) Validation of the identified Brat-binding motif using EMSAs. ^{32}P-labeled 15-mers (2.5 nM) encompassing the Brat consensus sequence or related sequences, as indicated below the autoradiogram, were incubated with increasing amounts of recombinant Brat-NHL, and complexes were analyzed by native gel electrophoresis.

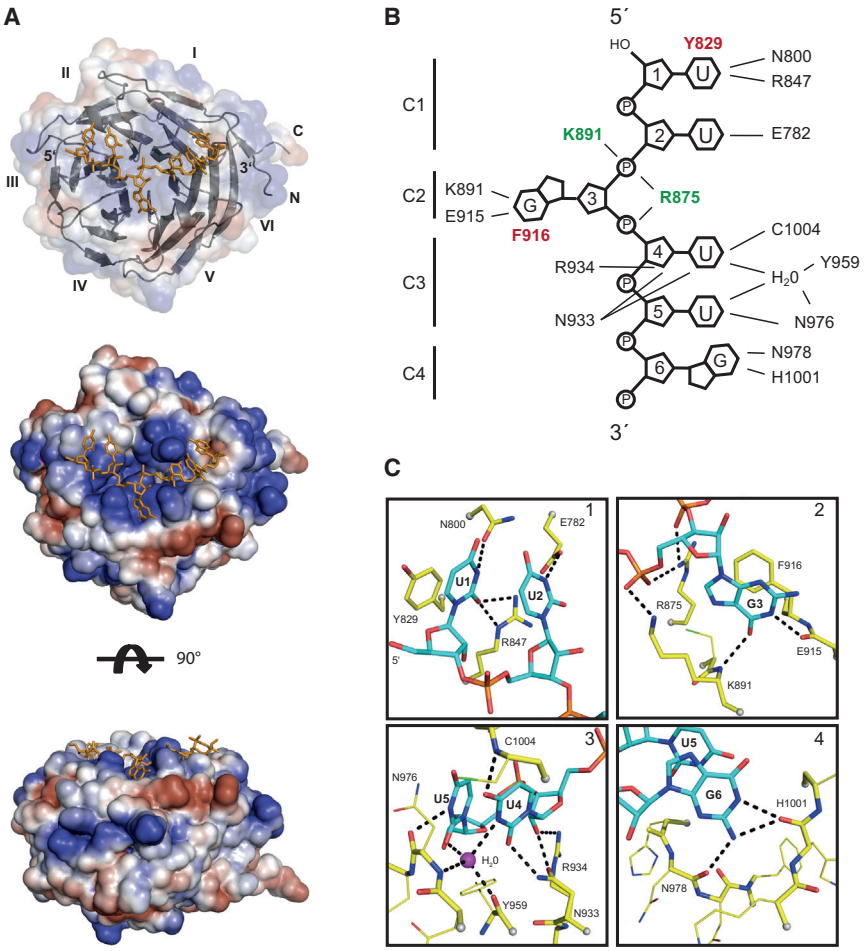

Figure 2. Structure of the *Drosophila* Brat-NHL Domain Bound to Its Consensus Motif RNA

(A) Structure model of the Brat-NHL domain bound to RNA. Top: model of the six-bladed β propeller of the NHL domain viewed from the top surface. The individual blades are numbered, and the bound RNA is shown as a stick representation. Center: electrostatic surface representation of the Brat-NHL top side with bound RNA. Bottom: side view of the complex with the electrostatic potential shown for the protein domain.

(B) Schematic of the protein:RNA contacts. Side chains forming stacking interactions to RNA bases are shown in red. Ionic interactions with the phosphate backbone of the RNA are indicated in green. Hydrogen bonds with the bases or sugars of the RNA are shown in black.

(C) Close-up view of the RNA binding pockets. RNA is shown in cyan, and protein residues are shown in yellow. Hydrogen bonds are marked by dashed lines. Side chains not interacting with the RNA are drawn as thin lines, and interacting side chains and backbone atoms are shown as thick lines and labeled. All chain cuts are marked with halos.

For a more detailed description of the molecular contacts and electron density maps, see Figure S2.

channel and exposes a positively charged top surface and a modestly negatively charged bottom surface. The RNA motif is bound in three pockets across the top surface, each located at the interface of two neighboring blades (Figure 2A). U1 and U2 stack onto each other and are bound in between blades II and III. G3 is flipped out and bound by blade IV and the loop connecting it to blade V, whereas the bases U4–G6 together occupy a binding cleft created by blades VI and I (Figure 2A).

All six RNA bases are specifically recognized by an intricate hydrogen bond network as well as π-stacking interactions between aromatic rings. In addition, the backbone phosphates of G3 and U4 are bound by ionic interactions with K891 and R875, which probably stabilizes the flipped-out conformation of G3 (Figure 2B).

The pyrimidine ring of U1 stacks against Y829 and is additionally bound by R847 and N800 via hydrogen bonds. The base of U1 and also the side chain of R847 show relatively weak electron density and elevated B factors, indicating some flexibility of this terminal residue. U2 stacks against U1 and is bound by the carboxyl group of E782 (Figure 2C, 1), further stabilizing the conformation.

G3 protrudes into a binding pocket on the opposite site of the RNA backbone, and there it is stacked against the phenyl ring of F916. The base identity is read out by two hydrogen bonds to the protein backbone. To discriminate purine from pyrimidine bases, ring position N1 contacts the peptide carbonyl of E915. The guanine-specific carbonyl group at ring position 6 forms a hydrogen bond to the backbone amide of K891. The equivalent position is occupied by an amino group in adenine that cannot form this contact (Figure 2C, 2).

U4 is the most tightly bound base of the recognition motif. The 2′OH of its ribose moiety forms two hydrogen bonds with side chains of N933 and R934, and both carbonyl groups of the uracil base are specifically recognized by hydrogen bonds to the side chain of N933 and the backbone amide of C1004. In addition, the nitrogen at ring position 3 binds to a tightly coordinated water molecule that is held in place by two hydrogen bonds to the protein backbone. The same water also contacts U5 at a ring carbonyl. The other carbonyl group of U5 and N3 of the pyrimidine ring forms hydrogen bonds to the backbone amide and side chain of N976 (Figure 2C, 3).

G6, the last nucleotide of the recognition site, binds to the peptide carbonyl of H1001 via N1 of the purine ring system and the amino group at position 2. This amino group, which is specific for the guanine base, additionally forms a hydrogen bond to another backbone carbonyl (N978; Figure 2C, 4).

Interestingly, a second Brat-NHL domain is bound to the oligo-U tail 3′ of the perfect recognition site in our structure, and these molecules build the asymmetric unit of the crystal (Figure S2). This arrangement allows a direct comparison of the interactions of an optimal versus a suboptimal recognition motif. U12 and

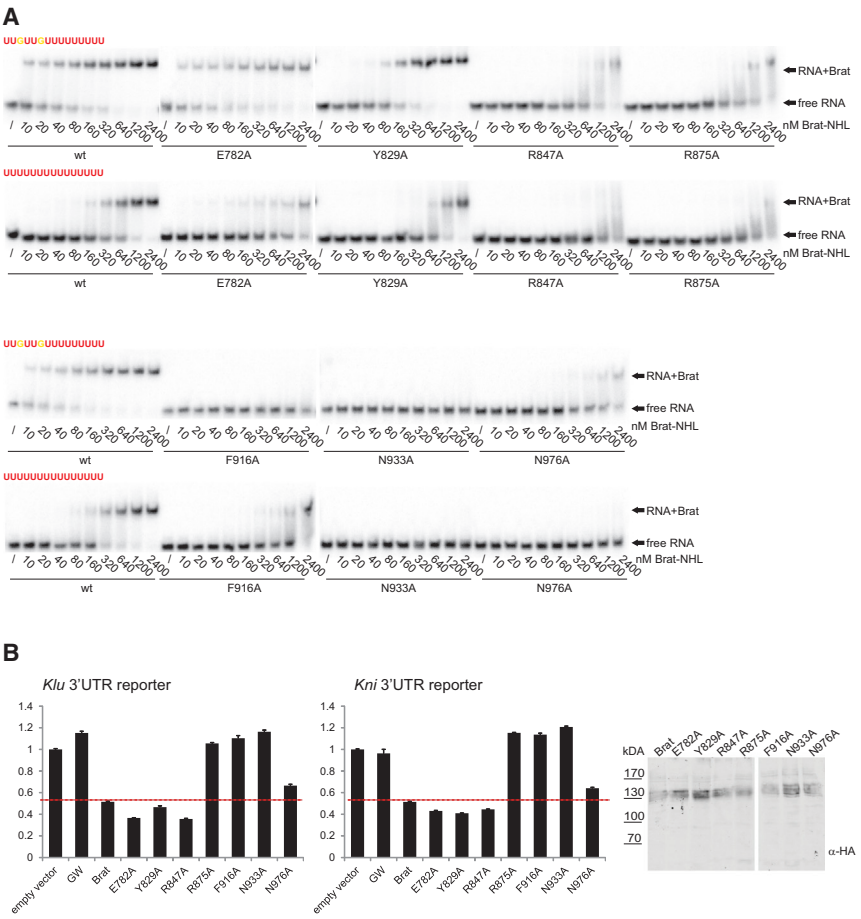

Figure 3. Validation of Protein-RNA Contacts

(A) RNA-binding of Brat-NHL and Brat-NHL RNA contact mutants. Increasing amounts of recombinant Brat-NHL (WT) or the indicated point mutants were incubated with ^{32}P-labeled 15-mers containing either the Brat consensus sequence or poly-U, as indicated, and complexes were analyzed by native gel electrophoresis.

(B) Reporter gene repression by Brat and Brat RNA contact mutants in Dmel2 cells. Left: Dmel2 cells were co-transfected with plasmids expressing firefly luciferase (FL)-*klu*-3′ UTR or FL-*kni*-3′ UTR reporter constructs (Figure 5B), the indicated HA fusion proteins, and a *Renilla* luciferase (RL) control plasmid. 48 hr after transfection, cells were lysed, and luciferase activities were measured. FL was normalized to RL, and values of normalized FL produced in the presence of an empty control vector were set to 1. Values represent the means of three independent experiments, each performed in triplicate, and error bars show SEM. Right: protein expression was analyzed by western blotting.

(C) Purity of recombinant Brat-NHL and Brat-NHL RNA contact mutants. Shown is Coomassie-stained SDS-PAGE of 5 μg of recombinant, purified Brat-NHL and the indicated Brat-NHL RNA contact mutants.

U13, which occupy positions equivalent to the tightly bound U4 and U5, form the same contacts with the protein and are clearly defined, with comparable B factors to their counterparts. In contrast, U11, which is flipped out into the pocket occupied by G3 in the other monomer, forms weaker stacking interactions with F916 and is not able to contact E915 at the bottom of the pocket. One ring carbonyl of the uracil base occupies an equivalent position to the guanine carbonyl and binds to the K891 peptide backbone in a similar manner. This interaction probably enables poly-U to serve as ligand for Brat-NHL. U14, which takes the position of G6, is only very weakly defined in the electron density because of its inability to form any of the hydrogen bonds observed for the guanine base.

Validation of Specific RNA-Protein Contacts

In our previous UV-cross-linking and mutagenesis studies we identified critical residues involved in RNA binding (Loedige et al., 2014) that are now confirmed by the crystal structure. These residues are located in the first and second binding pocket, namely Y829, R847 (pocket 1), R875, C890, K891, and F916 (pocket 2), and either directly interact with the bound RNA or are in close proximity. However, other residues that we have suggested to be involved in RNA binding do not contact the RNA directly in our structure.

For validation, we compared direct binding of wild-type (WT) Brat-NHL and several Brat-NHL variants mutated in the first (E782A, Y829A, and R847A), second (R875A and F916A), and third binding pocket (N933A and N976A) in EMSAs using either the perfect Brat consensus sequence or poly-U as ligand (Figure 3A). Additionally, these mutations were tested in the context of the full-length protein in reporter gene assays (Figure 3B).

Mutations of residues E782 and Y829 in the first binding pocket have a weak effect on the total affinity to RNA, consistent with the fewer protein-RNA contacts and higher flexibility in this region. Additionally, their ability to contact RNA is reflected by

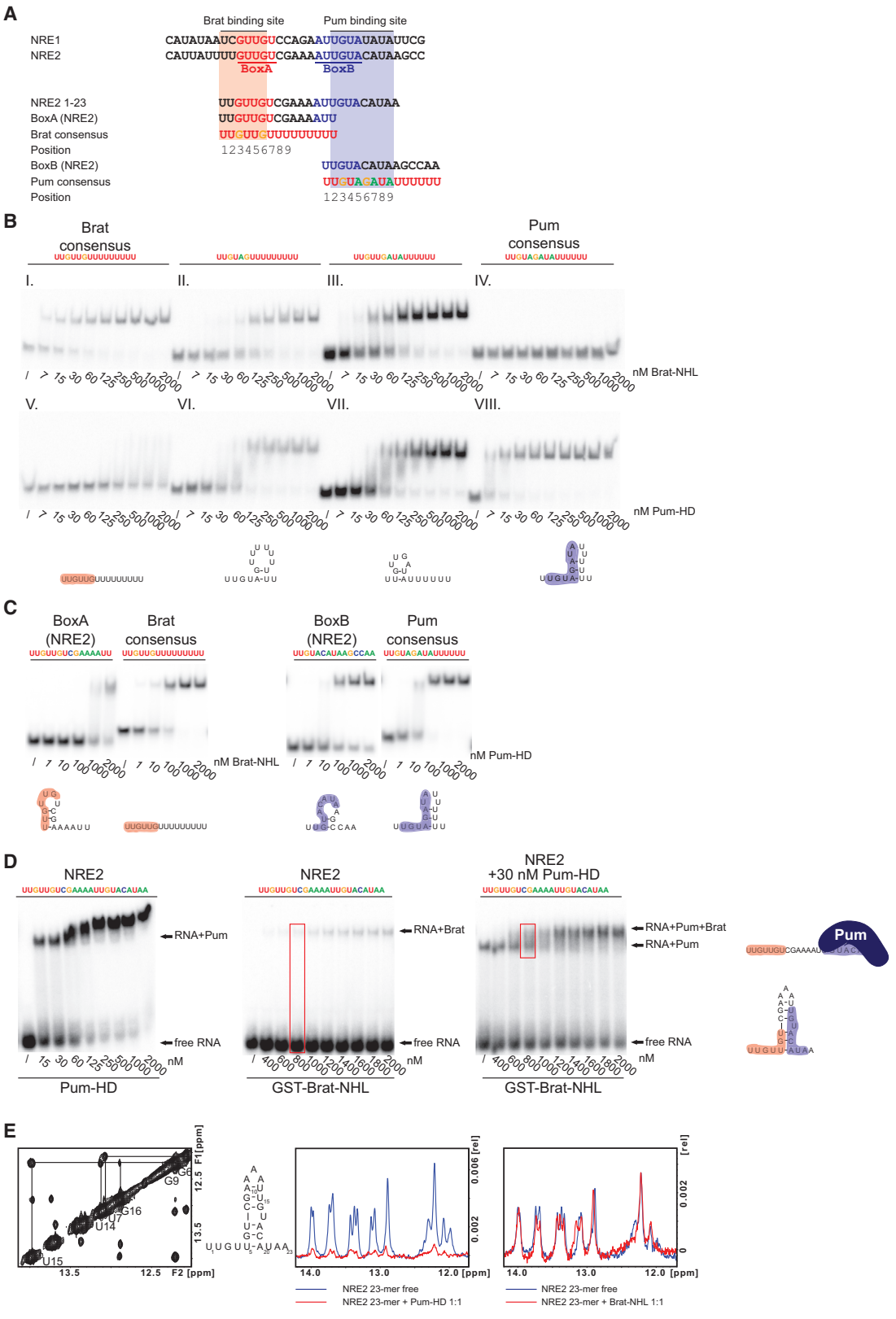

(legend on next page)

their capability to bring about reporter gene repression. In contrast, mutation of residues that constitute the second (R875A and F916A) and third (N933 and N976) binding pocket completely or almost completely abrogates Brat-NHL RNA binding. Consequently these mutants lost their ability to repress reporter genes or, in the case of N976A, show reduced activity, confirming the strong contribution of these residues to RNA binding. Only R847A, which forms hydrogen bonds with U1, behaved unexpectedly. Full-length BRAT R847A is still capable to repress reporter genes, indicating its association with target RNAs in vivo. However, in direct binding assays, Brat-NHL R847A showed almost no affinity to RNA. Circular dichroism (CD) spectroscopy (data not shown) revealed an identical folding of the secondary structure elements compared with the wild-type protein. On a gel filtration column, the elution volume is changed (data not shown), possibly indicating a difference in tertiary structure. This effect might be compensated in the context of the full-length protein, and, therefore, binding in EMSAs is lost because of partial mis-folding.

Uridine at Position 5 Discriminates a Brat from a Pum Consensus Sequence

Repression of the *hb* mRNA depends on sequence elements termed Nanos response elements (NREs), which are located in the 3′ UTR. Each NRE is composed of a BoxA and a BoxB site that overlap with the Brat and Pum binding sites, respectively (Figure 4A). Similar to Brat, RNA binding by Pum is sequence-specific, and an 8-nt motif, UGUANAUA (with N being any nucleotide), has been identified as the Pum consensus motif (Gerber et al., 2006). Interestingly, the Brat and Pum binding motifs bear some resemblance, with both motifs containing a central UGU, and, initially, the BoxA motif had been assumed to constitute a weak Pum binding site (Wang et al., 2002).

The identification of the Brat binding motif allows the examination of the molecular determinants that discriminate a Brat from a Pum site. To do so, we performed EMSAs analyzing the binding affinities of Brat-NHL or the Pum RBD (Pum homology domain [Pum HD]) to 15-mers encompassing either the Brat (I/V) or the Pum consensus (IV/VIII) or intermediates of the two sequences (Figure 4B). The exchange of three uridines at positions 5, 7, and 9 into adenosines converts the Brat consensus sequence into a Pum consensus sequence (Figure 4A). As expected, Brat-NHL binds the Brat consensus with high affinity (I, ~30 nM) but has no affinity for the Pum consensus (IV), whereas the Pum HD has high affinity for its consensus (VIII, ~10 nM) but binds only poorly to the Brat motif (V). Substitution of a single uridine at position 5 into an adenosine reduces the affinity of the 15-mer for Brat-NHL (II, >100 nM) while increasing the affinity for the Pum HD (VI). Exchange of two uridines at positions 7 and 9 into adenosines has a similar but less pronounced effect (III and VII), indicating that these positions distinguish Brat and Pum binding sites. Based on the Pum HD crystal structure, adenosines at these positions form hydrogen bonds and van der Waals interactions with the Pum HD, but these contacts are not made when adenosine is replaced by a smaller pyrimidine base, explaining the differences in binding affinities (Wang et al., 2002). In the case of Brat-NHL, the third binding pocket (Figure 2C) is perfectly suited to specifically accommodate uridines at positions 4 and 5, including most of the interactions with the protein backbone and side chains. This illustrates how distinction between similar motifs can be brought about and how both proteins are optimized for their motifs, to which they bind with high affinity. Interestingly, within our MEME-derived in vivo Brat-binding motif (Figure 1D), position 5 is the only position where no nucleotide other than uridine is found.

RNA Secondary Structure Reduces Brat-NHL Accessibility

In contrast to uridine at position 5, the uridines at positions 7 and 9 are not part of the Brat consensus motif and make no contact with the protein, indicating that other determinants must account for the observed affinity drop when these uridines are replaced by adenines (Figure 4B). Interestingly, the 15-mer containing the Brat consensus sequence is predicted to be linear by mfold (Zuker, 2003) (as are the 15-mers tested and shown in Figure 1F). In contrast, the Pum motif containing additional adenosines forms secondary structures (Figure 4B).

In EMSAs, Brat-NHL binds to a 15-mer encompassing the *hb* NRE2 BoxA site with low affinity but shows high affinity when the motif is embedded in a poly-U backbone (Figure 4C, left). Structure prediction revealed that the NRE2 BoxA forms secondary structures (Figure 4C, left), suggesting that the structural context of the Brat-binding motif affects binding affinities. In contrast to

Figure 4. Sequence and Structural Features Discriminate Brat and Pum Binding

(A) NRE RNA sequences and RNAs used in EMSAs. BoxA and BoxB sites are indicated with red and blue letters, respectively. Nucleotides bound by Brat and Pum are highlighted in light red or blue, respectively.

(B) Increasing amounts of recombinant Brat-NHL (I–IV) or the Pum HD (V–VIII) were incubated with ^{32}P-labeled 15-mers encompassing either the Brat consensus (I and V), the Pum consensus (IV and VIII), or intermediates of the two sequences (II, III, VI, and VII), as indicated, and complexes were analyzed by native gel electrophoresis. RNA structures as predicted by mfold are depicted below the respective autoradiograms.

(C) Structural features constrain Brat-NHL binding. Increasing amounts of Brat-NHL (left) or the Pum HD (right) were incubated with ^{32}P-labed 15-mers either encompassing the respective consensus sequence or with 15-mers covering the BoxA or the BoxB motif of the *hb* NRE2, respectively. Complexes were analyzed by native gel electrophoresis. RNA structures are depicted below the respective autoradiograms.

(D) Binding of the Pum HD to NRE2 facilitates subsequent Brat-NHL binding. Increasing amounts of the Pum HD (left) or GST-tagged Brat-NHL (center and right) were mixed with a ^{32}P-labeled 23-mer encompassing the *hb* NRE2, either alone (left and center) or pre-incubated with 30 nM Pum HD (right), and the resulting complexes were analyzed by native gel electrophoresis. GST-Brat-NHL preferentially bound to the NRE2 that was already bound by the Pum HD. The mfold predicted structure of the NRE2 is shown on the right. Note that GST-tagged Brat-NHL was used to better discriminate Brat-NHL-NRE2 from Pum-HD-NRE2 complexes.

(E) 2D imino nuclear Overhauser enhancement spectroscopy (NOESY) of NRE2 23-mer confirms RNA secondary structure (left). The assigned G-U base pair is indicated. The Pum HD, but not Brat-NHL, is able to melt RNA-RNA base-pairing. Imino peaks indicative of RNA base-pairing vanish upon titration of NRE2 with the Pum HD (left) but not by Brat-NHL (right).

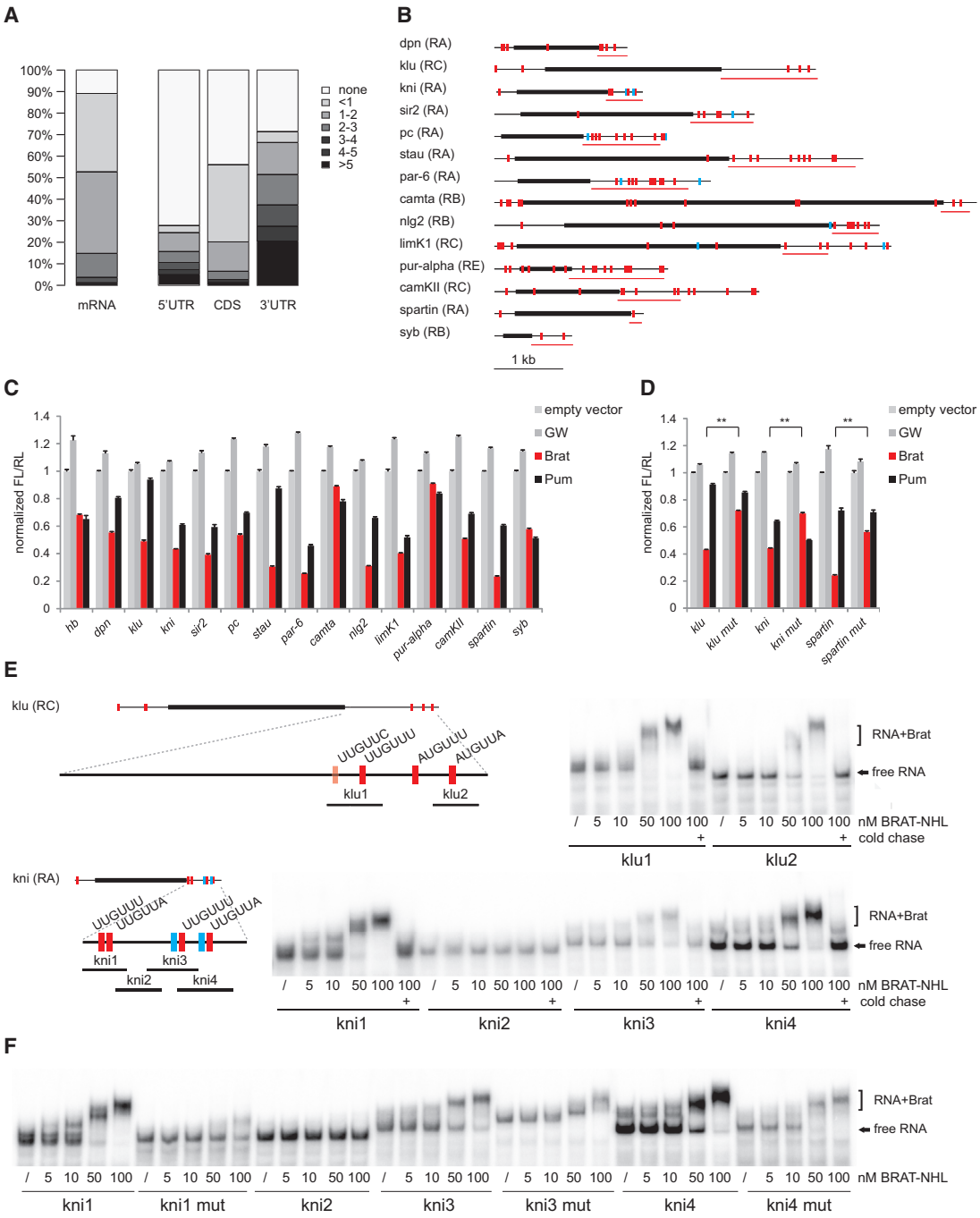

Figure 5. Repression and Direct Binding of Brat to mRNAs Identified by RIP-Chip

(A) The Brat consensus sequence is enriched within UTRs. For the 2,204 top-ranking Brat-RIP targets (log2FC > 1.5), the average number of Brat-binding sites per 1-kb sequence length was determined either for each transcript (mRNA) or for the 5′ UTR, the CDS, and the 3′ UTR individually.

(B) Schematic of transcripts selected for reporter gene assays. Gene names are given on the left, and the mRNA isoform depicted is indicated in parentheses. The CDS is shown as a thick black line and the 5′ and 3′ UTRs as thin black lines. Red boxes indicate consensus Brat-binding sites ([U/A]UGUU[A/U/G]), and blue boxes indicate consensus Pum sites (UGUANAUA). Indicated by thin red lines are the segments of the 3′ UTRs that were used to generate FL reporter constructs.

(C) Repression of potential Brat targeted 3′ UTRs in Dmel2 cells. Dmel2 cells were co-transfected with plasmids expressing the indicated FL-3′ UTR reporter constructs, an RL control, and either HA-tagged GW or Brat or Pum or an empty vector control, and reporter assays were performed as described in Figure 3B.

(D) Mutation of Brat-binding sites abrogates Brat-mediated repression. Reporter assays were performed as described in (C) with the indicated FL-3′ UTR reporter constructs or with constructs having all potential Brat-binding sites mutated. **$p < 0.01$.

(legend continued on next page)

Brat-NHL, the Pum HD binds its consensus sequence with high affinity despite RNA folding (Figure 4C, right).

Within the NREs, the Brat and Pum binding sites are in close proximity to each other, and we wondered whether a change in RNA secondary structure upon Pum binding to the BoxB site might change the folding of BoxA and, therefore, enable Brat binding. To address this question, we performed EMSAs using a radiolabeled 23-mer that encompasses the *hb* NRE2 sequence, including BoxA and BoxB sites (Figure 4D). As predicted by mfold, this RNA forms a hairpin structure, and nucleotides from both motifs are engaged in base-pairing (Figure 4D, schematic). The Pum HD binds the 23-mer with high affinity (~30 nM) (Figure 4D, left), whereas the affinity of Brat-NHL for this RNA is low (>2 μM) (Figure 4D, center). However, when NRE2 is pre-bound by the Pum HD, Brat-NHL binding is increased (Figure 4D, right). We made similar observations before using a longer, ~100-nt fragment of the *hb* mRNA (Loedige et al., 2014). To directly test whether titration of Brat-NHL or the Pum HD affects RNA folding, we performed nuclear magnetic resonance (NMR) experiments (Figure 4E). To stabilize the putative RNA secondary structure in vitro, the experiments were carried out at 5°C. A clear indication of nucleic acid base-pairing is NMR resonances in between relative frequencies of 10 and 15 ppm. Therefore, the presence of these signals confirms that the NRE2 23-mer is indeed structured. The number of cross-peaks indicates the formation of at least six base pairs (Figure 4E, left), which is in agreement with mfold prediction. However, additional diagonal imino peaks also indicate the possibility of multiple conformations or double strand formation. Addition of Brat-NHL up to a ratio of 2:1 (protein:RNA) did not decrease the intensity of imino signals, and only very small chemical shift changes could be observed, suggesting only weak, unspecific BRAT-NHL/RNA contacts (Figure 4E, right). In contrast, addition of the Pum HD decreased imino signal intensities already at a ratio of 0.3:1 (protein:RNA) and vanished completely upon reaching a ratio of 1:1 (Figure 4E, center). Therefore, the Pum HD not only binds to structured RNA but also affects its folding, possibly liberating the Brat-binding motif from secondary structures.

Notably, small-angle X-ray scattering (SAXS) analysis revealed that, within the context of the ~100-nt *hb* RNA, which contains two NREs, the Pum HD seems to be necessary for Brat-NHL to occupy both sites, supporting the model of structural RNA rearrangements by the Pum HD (Table S3; Figure S3).

To interrogate whether an NRE-like constellation is common, we searched the 3′ UTRs of our top-ranking Brat targets (log2 fold change [log2FC] > 1.5) for the presence of the Pum consensus (UGUANAUA). Of the 2,204 Brat-associated transcripts, 653 contain Pum consensus sites within their 3′ UTR. Of these, 290 have Brat and Pum binding sites less than 50 nt apart (Figure S3C), suggesting the possibility of an NRE-like regulation in these cases. Although a large number of our Brat targets carry a Pum motif, the Pum motif does not occur more frequently in the Brat targets than its reverse complement (Figure S3D), indicating that, for the majority of targets, Brat acts independently of Pum.

Brat Regulates a Number of Target Genes Implicated in Developmental Processes

Having elucidated the molecular details of the Brat-NHL RNA interaction, we went back to take a closer look at the Brat-mediated regulation of mRNAs that we identified as putative Brat targets (Figure 1B). We first determined the distribution of Brat-binding sites between UTRs and the coding sequence (CDS) within our top-ranking Brat targets (log2FC > 1.5) (Figure 5A). To account for differences in sequence length, we counted the average number of Brat-binding sites per kilobase, revealing a clear enrichment of Brat-binding sites within the 3′ UTR (Figure 5A).

During NB asymmetric cell divisions, Brat is segregated into the progenitor cell that is committed to differentiate. Here Brat downregulates NB-specific factors, important to drive differentiation. Although downregulation of *diminutive* by Brat has been shown to occur post-transcriptionally (Betschinger et al., 2006), direct mRNA binding and regulation by Brat as well as its NB-specific targets have not been reported. Among our Brat-associated mRNAs are numerous genes associated with NB self-renewal (Table S4). In addition, gene ontology (GO) analyses revealed a strong enrichment of genes with roles in synaptic transmission, neurotransmitter release, and membrane trafficking (Figure S4; Table S5), consistent with the regulatory roles of Brat in neuronal excitability, synaptic development, and axon maintenance that have been described previously (Marchetti et al., 2014; Muraro et al., 2008; Shi et al., 2013). Brat-targeted mRNAs important for early embryogenesis, such as *hb*, are not identified in this study because our epitope-tagged Brat is not expressed at this stage. (Of note, in the parallel study by Laver et al. (2015), different embryonic stages (prior to neuroblast specification) have been analyzed, and, therefore, distinct sets of mRNA targets have been identified.)

For further analysis, we selected candidates that are either associated with NB self-renewal (*dpn*, *klu* and *knirps* (*kni*), *sir2*, *polycomb* (*pc*), *stau*, and *par-6*) or candidates involved in synaptic regulation (*limkI*, *camKII*, or *pur-α*) to test their repression by Brat (Figure 5B). For reasons elucidated earlier, we also tested repression of these constructs by Pum. *hb* mRNA, known to be repressed by both Brat and Pum, served as a positive control. Reporter constructs were co-transfected with hemagglutinin (HA)-tagged Brat, Pum, or, as a negative control, Gawky (GW) into Dmel2 cells, and luciferase activity was measured 2 days post-transfection (Figure 5C). Under these conditions, expression of Brat led to repression of all but two of the tested reporters, demonstrating Brat-mediated regulation. Most of the reporters were also repressed by Pum, albeit weaker than observed for Brat, and repression of *klu* and *stau* was solely Brat-specific.

(E) Direct binding of Brat-NHL to *klu* and *kni* 3′ UTRs. Left: close-up view of the *klu* and *kni* 3′ UTRs. Indicated by short black lines (klu1-2 and kni1-4, respectively) are the ~150-nt-long fragments tested for direct Brat-NHL binding in the EMSAs shown on the right. Right: ^{32}P-labeled, ~150-nt-long fragments from the *klu* or *kni* 3′ UTR were incubated with increasing amounts of Brat-NHL and analyzed by native gel electrophoresis.
(F) Mutation of Brat-binding sites impairs direct Brat-NHL binding. EMSAs were performed as described in (E) with the indicated *kni* 3′ UTR fragments or with fragments having all Brat-binding sites mutated.

To further solidify our observations, we mutated the consensus Brat-binding sites from the *klu*, *kni*, and *spartin* 3′ UTRs and repeated the luciferase experiments (Figure 5D). In all three cases, mutation of the Brat-binding sites significantly reduced Brat-mediated repression, indicating that inhibition depends on the identified Brat-binding motif. Notably, mutation of the Brat-binding sites did not affect repression by Pum.

We next analyzed direct binding of the Brat-NHL domain to fragments of the *klu* and *kni* 3′ UTRs in EMSA experiments (Figure 5E). Because native gel electrophoresis restricts the length of RNAs that can be tested, we divided the 3′ UTRs into smaller, ~150-nt-long fragments (Figure 5E). Using this direct binding approach, we find that Brat-NHL binds to all tested 3′ UTR fragments that contain a Brat-binding site, whereas the fragment kni2, which lacks a consensus Brat-binding site, is not bound. Last, we repeated the experiment with *kni* 3′ UTR fragments in which all Brat-binding sites were mutated and observed that their mutation either completely abolished or at least reduced Brat binding to these fragments (Figure 5F), indicating that Brat binding is direct and mediated by the identified sequence motif.

Miranda Inhibits Brat RNA Binding

Segregation of Brat into differentiating daughter cells during asymmetric NB divisions depends on the adaptor protein Miranda (Mira) (Betschinger et al., 2006; Lee et al., 2006). During late pro-metaphase, Mira accumulates alongside its cargo proteins, including Brat, at the basal cortex of the dividing cell. After mitosis, Mira is rapidly degraded and, therefore, cargo proteins are released. The interaction between Brat and Mira is mediated by the NHL domain of Brat, and several residues on the top surface of the NHL domain are critical for the interaction (Lee et al., 2006). Interestingly, the Mira and RNA contact surfaces likely overlap, prompting us to investigate whether Mira might interfere with Brat RNA-binding.

To test this hypothesis, we performed reporter experiments. Plasmids expressing luciferase reporters containing the 3′ UTRs of NB-specific factors were transfected together with plasmids expressing NHA-tagged Brat and increasing amounts of Mira or LacZ (Figure 6B). As expected, all reporters were strongly repressed upon Brat expression (Figure 6B, red bars). Strikingly, Brat-mediated repression was strongly reduced when Mira, but LacZ, was co-expressed. When Brat was physically tethered to the RNA via boxB sites (Gehring et al., 2003), Mira had no effect, indicating that Mira does not affect Brat-mediated repression but RNA-binding of Brat.

It has been reported before that point mutations in the NHL domain of Brat, G774D and Y829A, destroy the interaction between Brat and Mira, whereas the Brat-NHL mutants R847A and R875A do not (Lee et al., 2006). Based on our crystal structure, residues Y829, R847, and R875 of the Brat-NHL domain contact the RNA; however, Brat Y829A and Brat R847A are still capable of bringing about reporter gene repression (Figure 3B). Therefore, we examined these Brat mutations in more detail (Figure 6C). The Mira binding-deficient mutants Brat-G774D and Brat-Y829A still repress *klu* and *kni*, but, in agreement with our model, this repression is not changed when Mira is co-expressed (Figure 6C). Moreover, Brat-R847A, which binds Mira, represses *klu* and *kni* expression, and, as expected, Mira co-transfection inhibits Brat-mediated reporter repression. Finally, we tested two Mira fragments for effects on Brat-mediated regulation (Figure 6D). Mira 181–432 does not contain the Brat binding region (Figure 6A), and, indeed, co-expression of this fragment does not affect Brat-mediated repression. Strikingly, Mira 344–568, which comprises the Brat-binding domain, inhibits Brat function comparable with WT Mira (Figure 6D). Based on these experiments, we suggest that Mira not only serves to correctly localize Brat to the basal cortex but also to inhibit Brat RNA-binding, preventing premature downregulation of Brat targets in NBs (Figure 6E).

Distinct RNA Binding Preferences of Different NHL Domains

Several TRIM-NHL proteins have been implicated in processes associated with RNA (Baltz et al., 2012; Castello et al., 2012; Chang et al., 2012; Kwon et al., 2013; Li et al., 2012; Neumüller et al., 2008; Schwamborn et al., 2009). We used RNAcompete to analyze the RNA binding preferences of TRIM-NHL proteins from diverse model organisms (Figure 7A). The NHL domains of human TRIM2, TRIM3, TRIM56, and TRIM71; *Drosophila* Brat, Wech, and Mei-P26; and *Caenorhabditis elegans* NCL-1, LIN-41, NHL-1, and NHL-2 were expressed and purified as glutathione S-transferase (GST) fusion proteins from either bacteria or insect cells and assayed using RNAcompete. Correlation between *Z* scores and motif logos from set A and set B indicated successful experiments for Brat, NCL-1, Mei-P26, and TRIM56 as well as for Wech, LIN-41, and TRIM71. The data for NHL-1, NHL-2, TRIM2, and TRIM3 did not pass internal quality control standards and could not be used to generate RNA-binding sites (data not shown).

Interestingly, RNAcompete revealed distinct RNA-binding preferences for the different NHL domains (Figure 7B). The three *Drosophila* TRIM-NHL proteins Brat, Wech, and Mei-P26 (~34% sequence identity within their NHL domains) show very different binding motifs, indicating that they associate with different RNA targets. The close Brat ortholog NCL-1, however, which shares 80% sequence identity within its NHL domain with Brat, recognizes the same RNA-binding motif as Brat. Likewise, the NHL domains of the three closely related TRIM-NHL proteins hsTRIM71, dmWech, and ceLIN-41 show highly similar binding preferences, suggesting that their structural conservation corresponds to recognition of similar RNA motifs. A multiple sequence alignment (Figure S5) reveals that close NHL homologs contain conserved residues at putative RNA contact position, whereas these residues are not generally conserved between distinct NHL domains.

To determine and compare binding affinities, we performed EMSAs with Brat-NHL, NCL-1-NHL, and Mei-P26-NHL and radiolabeled 15-mers that contained either the Brat and NCL-1 binding motif (UUGUUG or UUGUUA) or the Mei-P26 binding motif (UUUACA) as well as related sequences, including poly-U (Figure 7C). Confirming the RNAcompete results, NCL-1-NHL displayed an identical RNA-binding preference as Brat-NHL. In contrast, Mei-P26-NHL bound to the Mei-P26 consensus sequence (UUUACA) with high affinity but, because of their U-rich nature, also displayed high affinity to the other 15-mers tested, confirming that Mei-P26 binds U-rich stretches, as revealed by RNAcompete.

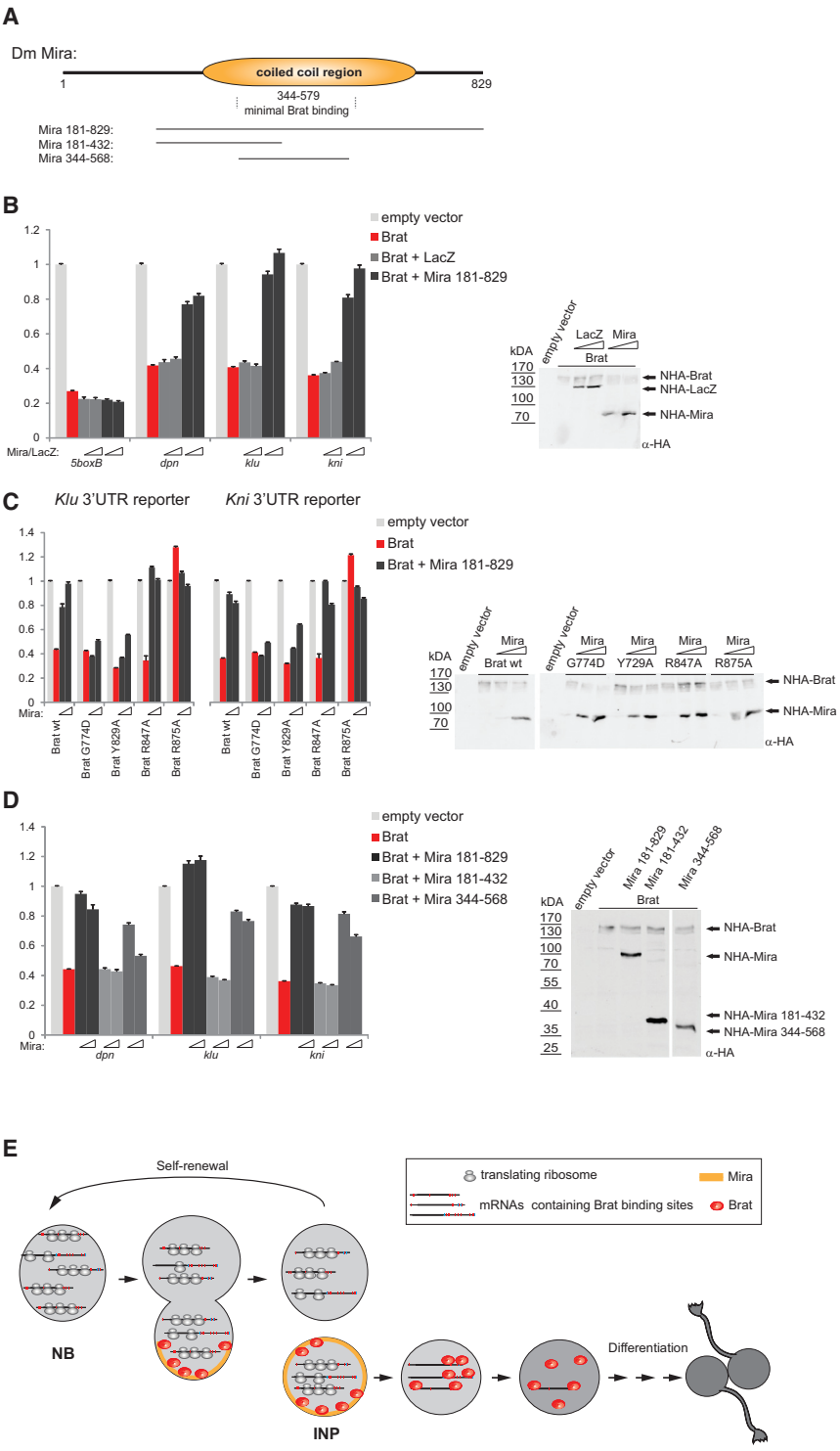

Figure 6. Miranda Inhibits Brat RNA Binding

(A) Schematic of dm Mira. The coiled-coil region is shown in yellow, and the boundaries of the minimal Brat-NHL-binding fragment are indicated. Shown below are the Mira constructs used in this study.

(B) Expression of Mira, but not of LacZ, prevents Brat-mediated repression. Left: Dmel2 cells were co-transfected with plasmids expressing the indicated FL-3′ UTR reporter constructs, NHA-tagged Brat, and increasing amounts of either NHA-tagged LacZ or Mira. Reporter assays were performed as described in Figure 3B. Right: protein expression was analyzed by western blotting.

(C) Point mutations that impair the interaction between Brat and Mira render Brat insensitive to Mira inhibition. Reporter assays were performed as described in (B), except that repression by WT Brat and the indicated point mutants was analyzed.

(D) Expression of the Mira minimal Brat-binding fragment is sufficient to inhibit Brat-mediated translational repression. Reporter assays were performed as described in (B), except that increasing amounts of the indicated Mira constructs were co-transfected.

(E) In dividing *Drosophila* NBs, interaction of Mira with the Brats NHL domain inhibits Brat RNA binding and directs Brat to the basal cell cortex. After mitosis, Mira is degraded, and Brat is released to bind and repress mRNAs of NB-specific factors important to drive differentiation.

DISCUSSION

The identification of binding sites of RBPs and the elucidation of how binding specificity and selectivity are brought about are key questions to understand post-transcriptional gene regulatory networks. Here, we report the identification of the target RNAs and the binding motif of the TRIM-NHL protein Brat. By solving the crystal structure of the Brat-NHL domain in complex with its consensus sequence, we provide molecular insights into how sequence specificity and selectivity in RNA binding by Brat-NHL is accomplished. Only a few RBDs, including RNA recognition motifs (RRMs), K homology (KH) domains, cold shock domains (CSDs), and DEAD box RNA helicases (Auweter et al., 2006), are well characterized, and their RNA specificity has been studied. The six-bladed β propeller of the NHL domain provides a compact platform (~47-Å diameter), and the RNA runs across the entire positively charged top surface. Sequence specificity is provided by surface complementary (three preformed binding clefts accommodate the six bases of the consensus motif) and base-specific hydrogen bonds to the protein main and side chain. Interestingly, all pockets are formed by two neighboring blades. It is therefore tempting to speculate that β propeller structures might be ideal platforms for generating sequence-specific RNA contacts, depending on the loops and side chains protruding into the inter-blade space. WD40 domains, which are highly abundant in eukaryotic proteomes (Stirnimann et al., 2010), fold into β propeller structures as well. Although their

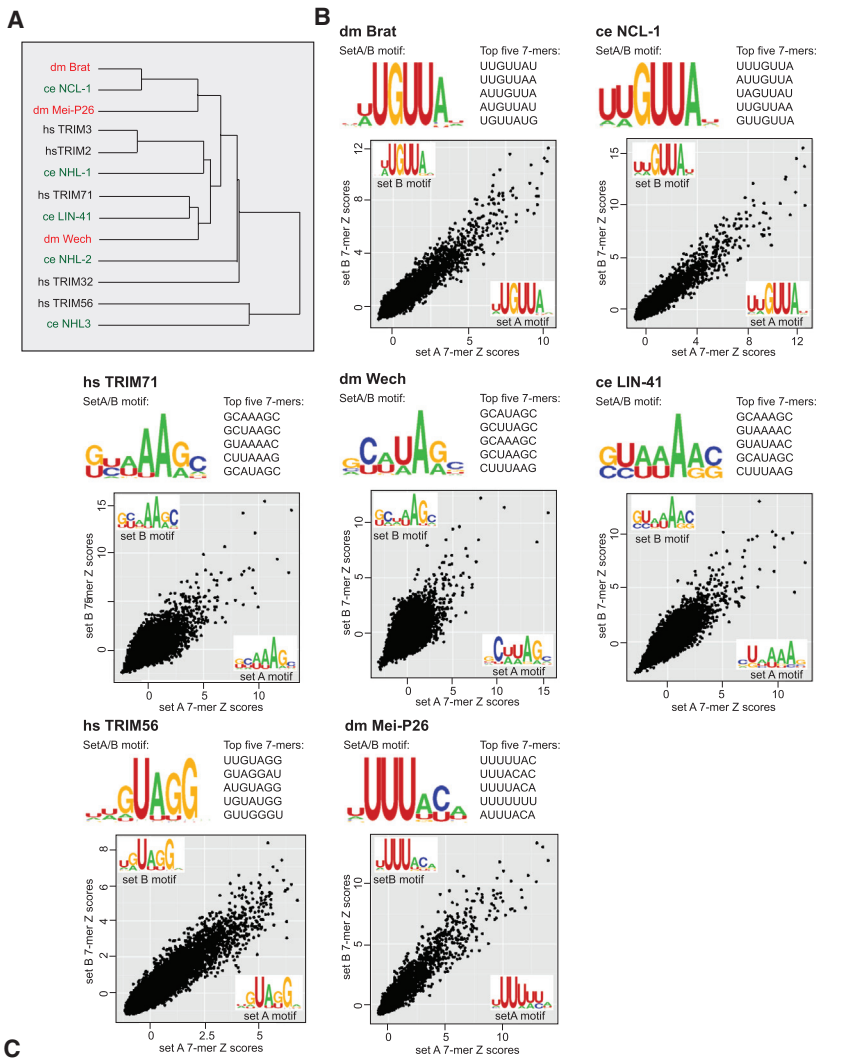

Figure 7. NHL Domains of Different TRIM-NHL Proteins Have Distinct RNA Binding Preferences

(A) Phylogeny of TRIM-NHL proteins. The average distance tree was calculated with BLOSUM62 using the NHL domains of human (hs), dm, and *C. elegans* (ce) TRIM-NHL proteins.

(B) Summary of RNAcompete experiments for the NHL domains of the indicated TRIM-NHL proteins. Depicted are the sequence logos of derived RNA-binding motifs, the top five high-scoring 7-mers, and the scatter plots, displaying *Z* scores and motifs for the two halves of the RNA pool (set A and set B) for each individual TRIM-NHL protein. Spots corresponding to enriched 7-mers are shown in the top right corner. Sequence logos were derived by aligning the top ten high-scoring 7-mers.

(C) Validation of identified binding motifs in EMSAs. Increasing amounts of purified Brat-NHL (top), NCL-1-NHL (center), and GST-tagged Mei-P26-NHL (bottom) were incubated with ^{32}P-labeld 15-mers encompassing either the Brat consensus (I), the Mei-P26 consensus (II), poly-U (III), or sequences used to validate the Brat consensus sequence (IV–VI).

direct mRNA binders (Baltz et al., 2012; Castello et al., 2012; Gerstberger et al., 2014; Kwon et al., 2013).

Using RNAcompete, we identified RNA-binding motifs for several members of the TRIM-NHL protein family, corroborating the hypothesis that TRIM-NHL proteins constitute a conserved family of RBPs. The observation that different TRIM-NHL proteins bind distinct sequence motifs suggests their association with different (m)RNA targets and their engagement in different biological processes. Evolutionary related NHL domains, however, use similar RNA-binding sites, indicating that the processes these TRIM-NHL proteins regulate might be conserved.

Brat-NHL binds single-stranded RNA, and its binding affinity seems to be impaired when nucleotides of the motif are engaged in RNA-RNA base-pairing, illustrating the importance of the structural context and target site accessibility. Even though the Pum HD is a single-stranded RBD as well, we still observe high-affinity binding when nucleotides of its motif base pair. We find that, within the context of the NRE, where Brat and Pum sites are in close proximity, Pum binding changes the RNA structure, resulting in a more accessible Brat-binding site. It should be noted that the observed binding mechanisms are in an in vitro setting. The secondary structure of the full-length 3′ UTR in vivo might be different and involve role in protein-protein interactions is well established, it is conceivable that WD40 domains are widespread sequence-specific RBDs. Supporting this idea, the WD40 domain of Gemin5 has been recognized as RBD interacting with small nuclear RNAs (snRNAs) (Lau et al., 2009), and recent large-scale screens have identified several WD40 domain containing proteins as

different regions as well as additional proteins being bound to the RNA. Nevertheless, for longer RNAs, the amount of secondary structure is probably larger and more dynamic.

Although we identify several examples of close proximity of Brat and Pum binding sites, we find no evidence for a general correlation of the two RBPs by computational analysis, indicating that, for the majority of targets, Brat acts independently of Pum. Nevertheless it seems conceivable that, in addition to Pum, other RBPs might affect Brat RNA binding activity as well. Close proximity of binding sites for two distinct RBPs can increase affinity and specificity as the cognate RNA sequence is elongated, as has been shown recently for the cooperative RNA recognition by Sxl and UNR binding to msl-2 mRNA (Hennig et al., 2014).

Brat's most prominent function is its role in repressing tumor formation in the larval brain. Brat-mutant brain tumors originate from immature progenitor cells of type II NBs that fail to downregulate self-renewal factors and revert into over-proliferating NBs (Janssens and Lee, 2014). Numerous genes associated with NB identity (Berger et al., 2012), potentially involved in tumor formation (Jüschke et al., 2013), or identified in a genome-wide RNAi screen for factors controlling NB self-renewal and differentiation (Neumüller et al., 2011) are on our list of Brat targets. These include, for example, the self-renewal transcription factors *dpn*, *klu*, and *kni* but also many genes that are still uncharacterized (Table S4). In cases where functional data are available, knockdown of most of the putative Brat targets leads to NB loss or decreased proliferation (Neumüller et al., 2011), phenotypes that would be expected for physiologically relevant Brat targets. Here we provide a molecular and structural understanding of how Brat mediates the downregulation of these NB-specific factors.

Asymmetric segregation of Brat into progenitor cells is accomplished by the adaptor protein Mira (Betschinger et al., 2006; Lee et al., 2006), and we show that Mira not only ensures correct segregation of Brat but also inhibits Brat function by preventing Brat RNA binding. This provides an elegant mechanism to have sufficient Brat available after cytokinesis when Mira is degraded but to prevent pre-mature downregulation of NB-specific factors in the NB (Figure 6E).

In addition to NB-specific factors, our list of Brat-associated mRNAs contains numerous genes characteristic for postmitotic neurons, including the known Brat target para, which encodes a voltage-gated Na^+ channel (Muraro et al., 2008). Brat is expressed in mature neurons and has been reported to regulate membrane excitability, synaptic size (Shi et al., 2013), and axon maintenance (Marchetti et al., 2014). Strikingly, gene ontology analysis of the Brat targets reveals a strong enrichment of categories associated with synaptic transmission, neurotransmitter regulation, secretion, and transport, and many Brat targets encode for proteins that localize to the plasma membrane and/or synaptic vesicle, including many ion channels and membrane-bound transporters. This strongly suggests that Brat regulates membrane-associated processes and might be involved in mRNA sorting and/or localization, a function that has not been described previously. In agreement with a function for brain-specific TRIM-NHL proteins in mRNA localization is the identification of the mammalian Brat orthologs TRIM2 and TRIM3 as components of mRNA transport granules (Kanai et al., 2004), their association with kinesin and myosin motor proteins (Labonté et al., 2013; Yan et al., 2005), and their enrichment in synaptic fractions, although their association with RNA still needs to be established. TRIM-NHL proteins have been implicated in the control of cell fate decisions in various tissues and across species (Chang et al., 2012; Chen et al., 2014; Li et al., 2012; Neumüller et al., 2008; Schwamborn et al., 2009; Slack et al., 2000; Worringer et al., 2014). Therefore, conferring robustness and directionality to cell fate decisions through mRNA regulation might be a common mechanism of TRIM-NHL protein action.

EXPERIMENTAL PROCEDURES

Fly Strains

To ubiquitously express FLAG-myc-tagged Brat in wild-type *Drosophila* embryos, virgins of da::GAL4 (no. 5460, obtained from the Bloomington *Drosophila* Stock Center) and UAS::FLAG-myc-Brat males (Shi et al., 2013) were mated at 25°C. Embryos were harvested after 24 hr.

Crystallization and Structure Determination

The Brat-NHL/RNA complex was formed by incubating the purified Brat-NHL domain with an equimolar amount of in vitro-transcribed consensus front RNA for 15 min on ice. The mixture was subsequently applied to a HiPrep Superdex 75 26/60 column equilibrated in 20 mM 4-(2-hydroxyethyl)-1-piperazineethanesulfonic acid (HEPES) (pH 7.5), 150 mM NaCl, and 1 mM DTT, and complex-containing fractions were pooled and concentrated to 2.6 mg/ml. After sparse matrix screening, one single crystallization condition containing 2 M ammonium sulfate, 5% polyethylene glycol 400, and 100 mM 2-(*N*-morpholino)ethanesulfonic acid (MES) (pH 6.5) could be identified, resulting in crystals suitable for X-ray diffraction. Crystals were taken out of the condition and directly frozen in liquid nitrogen without further treatment. X-ray diffraction experiments were carried out at the Beamline 14.2 of the Berliner Elektronenspeicherring für Synchrotronstrahlung (BESSY) synchrotron (Helmholtz-Zentrum Berlin). Native data could be obtained up to 2.3-Å resolution. Dataset statistics are given in Table S2. The dataset was processed using XDS (Kabsch, 2010), and initial phases were obtained from molecular replacement using Phaser and a search model based on the structure of the unliganded Brat-NHL domain (PDB code 1Q7F) (Edwards et al., 2003). A structure model was manually built in COOT (Emsley and Cowtan, 2004) and refinement was performed with PHENIX.refine (Adams et al., 2010) using non-crystallographic symmetry (NCS) restraints and simulated annealing. The model of the bound RNA was improved by rebuilding using ERRASER (Chou et al., 2013). Refinement and model statistics are given in Table S2.

ACCESSION NUMBERS

The accession number for the coordinates and structure factors reported in this paper is PDB: 4ZLR and microarray data is available in the Gene Expression Omnibus database under accession numbers GEO: GSE71663 and GSE73000.

SUPPLEMENTAL INFORMATION

Supplemental Information includes Supplemental Experimental Procedures, five figures, and seven tables and can be found with this article online at http://dx.doi.org/10.1016/j.celrep.2015.09.068.

AUTHOR CONTRIBUTIONS

I.L. designed the study, produced samples, performed experiments, interpreted data, and wrote the manuscript. L.J., T.T., and N.T. produced samples, crystallized the complex, solved the structure, and wrote the paragraph

describing the structure. D.R. performed the RNAcompete assay (with protein prepared by I.L. and M.S.). M.S. designed the study, produced samples, and interpreted data. J.H. designed experiments, performed NMR and SAXS, interpreted data, and wrote the paragraph describing these experiments. K.B.C. analyzed the RNAcompete data. Q.M. and T.R.H. supervised D.R. and K.B.C. J.C.E. performed bioinformatic analyses. M.P.K. designed experiments, interpreted data, and supervised all fly work. G.M. interpreted data, wrote the manuscript, and secured funding.

ACKNOWLEDGMENTS

We thank Marina Chekulaeva and Julien Bethune for critically reading the manuscript. We thank Corinna Friederich, Sigrun Ammon, Melanie Royer for excellent technical support and Arnab Sen and Cornelia Bleyl for introduction to fly work. We are grateful to Marina Chekulaeva, Helge Grosshans, Jan Medenbach, Magdalene Rausch, Spencer Whitney, and Yong Zhang for reagents. We thank the Helmholtz-Zentrum Berlin for the allocation of synchrotron radiation beam time and the staff of the HZB MX group for support during data acquisition and gratefully acknowledge Prof. Michael Sattler and the Bavarian NMR Center (BNMRZ) for NMR/SAXS measurement time. Our research is supported by grants from the Deutsche Forschungsgemeinschaft (SFB 960 and FOR2127 to G.M. and KR3901/1-2 and KR3901/2-1 to M.P.K.), the European Research Council (242792 "sRNAs" and ITN RNATrain), the Bavarian Genome Research Network (BayGene), the Bavarian Systems-Biology Network (BioSysNet), and a CIHR operating grant (to T.R.H. and Q.D.M.).

Received: May 2, 2015
Revised: July 31, 2015
Accepted: September 24, 2015
Published: October 29, 2015

REFERENCES

Adams, P.D., Afonine, P.V., Bunkóczi, G., Chen, V.B., Davis, I.W., Echols, N., Headd, J.J., Hung, L.W., Kapral, G.J., Grosse-Kunstleve, R.W., et al. (2010). PHENIX: a comprehensive Python-based system for macromolecular structure solution. Acta Crystallogr. D Biol. Crystallogr. *66*, 213–221.

Auweter, S.D., Oberstrass, F.C., and Allain, F.H. (2006). Sequence-specific binding of single-stranded RNA: is there a code for recognition? Nucleic Acids Res. *34*, 4943–4959.

Bailey, T.L., and Elkan, C. (1994). Fitting a mixture model by expectation maximization to discover motifs in biopolymers. Proc. Int. Conf. Intell. Syst. Mol. Biol. *2*, 28–36.

Baltz, A.G., Munschauer, M., Schwanhäusser, B., Vasile, A., Murakawa, Y., Schueler, M., Youngs, N., Penfold-Brown, D., Drew, K., Milek, M., et al. (2012). The mRNA-bound proteome and its global occupancy profile on protein-coding transcripts. Mol. Cell *46*, 674–690.

Berger, C., Harzer, H., Burkard, T.R., Steinmann, J., van der Horst, S., Laurenson, A.S., Novatchkova, M., Reichert, H., and Knoblich, J.A. (2012). FACS purification and transcriptome analysis of Drosophila neural stem cells reveals a role for Klumpfuss in self-renewal. Cell Rep. *2*, 407–418.

Betschinger, J., Mechtler, K., and Knoblich, J.A. (2006). Asymmetric segregation of the tumor suppressor brat regulates self-renewal in Drosophila neural stem cells. Cell *124*, 1241–1253.

Brand, A.H., and Livesey, F.J. (2011). Neural stem cell biology in vertebrates and invertebrates: more alike than different? Neuron *70*, 719–729.

Castello, A., Fischer, B., Eichelbaum, K., Horos, R., Beckmann, B.M., Strein, C., Davey, N.E., Humphreys, D.T., Preiss, T., Steinmetz, L.M., et al. (2012). Insights into RNA biology from an atlas of mammalian mRNA-binding proteins. Cell *149*, 1393–1406.

Chang, H.M., Martinez, N.J., Thornton, J.E., Hagan, J.P., Nguyen, K.D., and Gregory, R.I. (2012). Trim71 cooperates with microRNAs to repress Cdkn1a expression and promote embryonic stem cell proliferation. Nat. Commun. *3*, 923.

Chen, G., Kong, J., Tucker-Burden, C., Anand, M., Rong, Y., Rahman, F., Moreno, C.S., Van Meir, E.G., Hadjipanayis, C.G., and Brat, D.J. (2014). Human Brat ortholog TRIM3 is a tumor suppressor that regulates asymmetric cell division in glioblastoma. Cancer Res. *74*, 4536–4548.

Chou, F.C., Sripakdeevong, P., Dibrov, S.M., Hermann, T., and Das, R. (2013). Correcting pervasive errors in RNA crystallography through enumerative structure prediction. Nat. Methods *10*, 74–76.

Edwards, T.A., Wilkinson, B.D., Wharton, R.P., and Aggarwal, A.K. (2003). Model of the brain tumor-Pumilio translation repressor complex. Genes Dev. *17*, 2508–2513.

Emsley, P., and Cowtan, K. (2004). Coot: model-building tools for molecular graphics. Acta Crystallogr. D Biol. Crystallogr. *60*, 2126–2132.

Gehring, N.H., Neu-Yilik, G., Schell, T., Hentze, M.W., and Kulozik, A.E. (2003). Y14 and hUpf3b form an NMD-activating complex. Mol. Cell *11*, 939–949.

Gerber, A.P., Luschnig, S., Krasnow, M.A., Brown, P.O., and Herschlag, D. (2006). Genome-wide identification of mRNAs associated with the translational regulator PUMILIO in Drosophila melanogaster. Proc. Natl. Acad. Sci. USA *103*, 4487–4492.

Gerstberger, S., Hafner, M., and Tuschl, T. (2014). A census of human RNA-binding proteins. Nat. Rev. Genet. *15*, 829–845.

Gómez-López, S., Lerner, R.G., and Petritsch, C. (2014). Asymmetric cell division of stem and progenitor cells during homeostasis and cancer. Cell. Mol. Life Sci. *71*, 575–597.

Hennig, J., Militti, C., Popowicz, G.M., Wang, I., Sonntag, M., Geerlof, A., Gabel, F., Gebauer, F., and Sattler, M. (2014). Structural basis for the assembly of the Sxl-Unr translation regulatory complex. Nature *515*, 287–290.

Janssens, D.H., and Lee, C.Y. (2014). It takes two to tango, a dance between the cells of origin and cancer stem cells in the Drosophila larval brain. Semin. Cell Dev. Biol. *28*, 63–69.

Jüschke, C., Dohnal, I., Pichler, P., Harzer, H., Swart, R., Ammerer, G., Mechtler, K., and Knoblich, J.A. (2013). Transcriptome and proteome quantification of a tumor model provides novel insights into post-transcriptional gene regulation. Genome Biol. *14*, r133.

Kabsch, W. (2010). Xds. Acta Crystallogr. D Biol. Crystallogr. *66*, 125–132.

Kanai, Y., Dohmae, N., and Hirokawa, N. (2004). Kinesin transports RNA: isolation and characterization of an RNA-transporting granule. Neuron *43*, 513–525.

Knoblich, J.A. (2010). Asymmetric cell division: recent developments and their implications for tumour biology. Nat. Rev. Mol. Cell Biol. *11*, 849–860.

Kwon, S.C., Yi, H., Eichelbaum, K., Föhr, S., Fischer, B., You, K.T., Castello, A., Krijgsveld, J., Hentze, M.W., and Kim, V.N. (2013). The RNA-binding protein repertoire of embryonic stem cells. Nat. Struct. Mol. Biol. *20*, 1122–1130.

Labonté, D., Thies, E., Pechmann, Y., Groffen, A.J., Verhage, M., Smit, A.B., van Kesteren, R.E., and Kneussel, M. (2013). TRIM3 regulates the motility of the kinesin motor protein KIF21B. PLoS ONE *8*, e75603.

Lau, C.K., Bachorik, J.L., and Dreyfuss, G. (2009). Gemin5-snRNA interaction reveals an RNA binding function for WD repeat domains. Nat. Struct. Mol. Biol. *16*, 486–491.

Laver, J.D., Li, X., Ray, D., Cook, K.B., Hahn, N.A., Nabeel-Shah, S., Kekis, M., Luo, H., Marsolais, A.J., Fung, K.Y., et al. (2015). Brain tumor is a sequence-specific RNA-binding protein that directs maternal mRNA clearance during the Drosophila maternal-to-zygotic transition. Genome Biol. *16*, 94.

Lee, C.Y., Wilkinson, B.D., Siegrist, S.E., Wharton, R.P., and Doe, C.Q. (2006). Brat is a Miranda cargo protein that promotes neuronal differentiation and inhibits neuroblast self-renewal. Dev. Cell *10*, 441–449.

Li, Y., Maines, J.Z., Tastan, O.Y., McKearin, D.M., and Buszczak, M. (2012). Mei-P26 regulates the maintenance of ovarian germline stem cells by promoting BMP signaling. Development *139*, 1547–1556.

Liu, Y., Raheja, R., Yeh, N., Ciznadija, D., Pedraza, A.M., Ozawa, T., Hukkelhoven, E., Erdjument-Bromage, H., Tempst, P., Gauthier, N.P., et al. (2014). TRIM3, a tumor suppressor linked to regulation of p21(Waf1/Cip1.). Oncogene *33*, 308–315.

Loedige, I., Stotz, M., Qamar, S., Kramer, K., Hennig, J., Schubert, T., Löffler, P., Längst, G., Merkl, R., Urlaub, H., and Meister, G. (2014). The NHL domain of BRAT is an RNA-binding domain that directly contacts the hunchback mRNA for regulation. Genes Dev. *28*, 749–764.

Marchetti, G., Reichardt, I., Knoblich, J.A., and Besse, F. (2014). The TRIM-NHL protein Brat promotes axon maintenance by repressing src64B expression. J. Neurosci. *34*, 13855–13864.

Muraro, N.I., Weston, A.J., Gerber, A.P., Luschnig, S., Moffat, K.G., and Baines, R.A. (2008). Pumilio binds para mRNA and requires Nanos and Brat to regulate sodium current in Drosophila motoneurons. J. Neurosci. *28*, 2099–2109.

Murata, Y., and Wharton, R.P. (1995). Binding of pumilio to maternal hunchback mRNA is required for posterior patterning in Drosophila embryos. Cell *80*, 747–756.

Neumüller, R.A., Betschinger, J., Fischer, A., Bushati, N., Poernbacher, I., Mechtler, K., Cohen, S.M., and Knoblich, J.A. (2008). Mei-P26 regulates microRNAs and cell growth in the Drosophila ovarian stem cell lineage. Nature *454*, 241–245.

Neumüller, R.A., Richter, C., Fischer, A., Novatchkova, M., Neumüller, K.G., and Knoblich, J.A. (2011). Genome-wide analysis of self-renewal in Drosophila neural stem cells by transgenic RNAi. Cell Stem Cell *8*, 580–593.

Ray, D., Kazan, H., Chan, E.T., Peña Castillo, L., Chaudhry, S., Talukder, S., Blencowe, B.J., Morris, Q., and Hughes, T.R. (2009). Rapid and systematic analysis of the RNA recognition specificities of RNA-binding proteins. Nat. Biotechnol. *27*, 667–670.

Ray, D., Kazan, H., Cook, K.B., Weirauch, M.T., Najafabadi, H.S., Li, X., Gueroussov, S., Albu, M., Zheng, H., Yang, A., et al. (2013). A compendium of RNA-binding motifs for decoding gene regulation. Nature *499*, 172–177.

Sardiello, M., Cairo, S., Fontanella, B., Ballabio, A., and Meroni, G. (2008). Genomic analysis of the TRIM family reveals two groups of genes with distinct evolutionary properties. BMC Evol. Biol. *8*, 225.

Schwamborn, J.C., Berezikov, E., and Knoblich, J.A. (2009). The TRIM-NHL protein TRIM32 activates microRNAs and prevents self-renewal in mouse neural progenitors. Cell *136*, 913–925.

Schwanhäusser, B., Busse, D., Li, N., Dittmar, G., Schuchhardt, J., Wolf, J., Chen, W., and Selbach, M. (2011). Global quantification of mammalian gene expression control. Nature *473*, 337–342.

Shi, W., Chen, Y., Gan, G., Wang, D., Ren, J., Wang, Q., Xu, Z., Xie, W., and Zhang, Y.Q. (2013). Brain tumor regulates neuromuscular synapse growth and endocytosis in Drosophila by suppressing mad expression. J. Neurosci. *33*, 12352–12363.

Slack, F.J., and Ruvkun, G. (1998). A novel repeat domain that is often associated with RING finger and B-box motifs. Trends Biochem. Sci. *23*, 474–475.

Slack, F.J., Basson, M., Liu, Z., Ambros, V., Horvitz, H.R., and Ruvkun, G. (2000). The lin-41 RBCC gene acts in the C. elegans heterochronic pathway between the let-7 regulatory RNA and the LIN-29 transcription factor. Mol. Cell *5*, 659–669.

Slaidina, M., and Lehmann, R. (2014). Translational control in germline stem cell development. J. Cell Biol. *207*, 13–21.

Sonoda, J., and Wharton, R.P. (2001). Drosophila Brain Tumor is a translational repressor. Genes Dev. *15*, 762–773.

Stirnimann, C.U., Petsalaki, E., Russell, R.B., and Müller, C.W. (2010). WD40 proteins propel cellular networks. Trends Biochem. Sci. *35*, 565–574.

Wang, X., McLachlan, J., Zamore, P.D., and Hall, T.M. (2002). Modular recognition of RNA by a human pumilio-homology domain. Cell *110*, 501–512.

Worringer, K.A., Rand, T.A., Hayashi, Y., Sami, S., Takahashi, K., Tanabe, K., Narita, M., Srivastava, D., and Yamanaka, S. (2014). The let-7/LIN-41 pathway regulates reprogramming to human induced pluripotent stem cells by controlling expression of prodifferentiation genes. Cell Stem Cell *14*, 40–52.

Yan, Q., Sun, W., Kujala, P., Lotfi, Y., Vida, T.A., and Bean, A.J. (2005). CART: an Hrs/actinin-4/BERP/myosin V protein complex required for efficient receptor recycling. Mol. Biol. Cell *16*, 2470–2482.

Ye, J., and Blelloch, R. (2014). Regulation of pluripotency by RNA binding proteins. Cell Stem Cell *15*, 271–280.

Zuker, M. (2003). Mfold web server for nucleic acid folding and hybridization prediction. Nucleic Acids Res. *31*, 3406–3415.